International Journal of Computer Assisted Radiology and Surgery manuscript No.
(will be inserted by the editor)

FCNN-based axon segmentation for convection-enhanced delivery optimization

Marco Vidotto · Elena De Momi · Michele Gazzara · Leonardo S. Mattos · Giancarlo Ferrigno · Sara Moccia

Received: date / Accepted: date

Abstract Purpose Glioblastoma-multiforme (GBM) treatment is a challenging task in clinical oncology. Convection Enhanced Delivery (CED) is showing encouraging but still suboptimal results due to drug leakages. Numerical models can predict drug distribution within the brain, but require retrieving brain physical properties, such as the axon diameter distribution (ADD), through axon architecture analysis. The goal of this work was to provide an automatic, accurate and fast method for axon segmentation in electronic-microscopy images based on fully convolutional neural network (FCNN) as to allow automatic ADD computation. **Methods** The segmentation was performed using a residual FCNN inspired by U-Net and Resnet. The FCNN training was performed exploiting mini-batch gradient descent and the Adam optimizer. The Dice coefficient was chosen as loss function. **Results** The proposed segmentation method achieved results comparable with already existing methods for axon segmentation in terms of Information Theoretic Scoring (0.98%) with a faster training (5 hours on the deployed GPU) and without requiring heavy post-processing (testing time was 0.2 s with a non-optimized code). The ADDs computed from the segmented and ground-truth images were statistically equivalent. **Conclusions** The algorithm proposed in this work allowed fast and accurate axon segmentation and ADD computation, showing promising performance for brain micro-structure analysis for CED delivery optimization.

M. Vidotto, M. Gazzara, G. Ferrigno and E. De Momi
Department of Electronics, Information and Bioengineering (DEIB), Politecnico di Milano
Piazza Leonardo da Vinci, 32, 20133 Milano (MI), Italy
E-mail: marco.vidotto@polimi.it

L. S. Mattos
Department of Advanced Robotics (ADVR), Istituto Italiano di Tecnologia
via Morego 30, 16136 Genoa (GE), Italy

S. Moccia
Department of Information Engineering (DII), Universitá Politecnica delle Marche
via Brecce Bianche, 12, 60131 Ancona (AN), Italy
Department of Advanced Robotics (ADVR), Istituto Italiano di Tecnologia
via Morego 30, 16136 Genoa (GE), Italy

Keywords Axon segmentation · electron microscopy · deep learning · convection-enhanced delivery · glioblastoma

1 Introduction

Gliomas are the most common brain tumors (40% of brain tumors [7]) and glioblastoma multiforme (GBM) is the most common and malignant one, accounting for 51% of gliomas [21].

Nowadays, GBM treatment is one of the most challenging tasks in clinical oncology. Despite the variety of modern therapies, GBM is still a deadly disease with extremely poor prognosis and median survival of 15 months from diagnosis [38]. The three main therapeutic approaches are surgical resection, radiation therapy and chemotherapy [15]. A high grade of GBM infiltration does not allow complete surgical resection and thus relapses occur [17]. Several risk factors and restrictions are associated with radiation therapy, including radiation necrosis, permanent radiation-induced neuronal damage and radio-resistance [15]. The biggest limitation in chemotherapeutic treatment is related to the blood-brain-barrier (BBB), which limits the spreading of the most common chemotherapeutic agents [19].

An alternative treatment procedure, called convection enhanced delivery (CED), has shown encouraging results in the last years [35]. In CED, a pharmacological agent is injected directly into the brain tissue by means of a catheter positioned in the target cancerous region, through a hole in the scalp. Drug spreading is driven by both a positive pressure and a diffusion gradient, allowing CED to overcome the main problems related to BBB [6, 10, 18].

Despite the encouraging results, it is widely accepted in the clinical literature that CED outcome is still suboptimal due to two main problems. The first is related to the choice of the optimal catheter design and the infusate backflow [45, 4]. The second deals with leakages within the substrate at the point of delivery and limited drug distribution [3, 36]. This paper specifically focuses on the second problem.

Drug distribution is controlled by drug infusion parameters, such as flow rate and infusion duration [42, 35]. A way to optimize the infusion parameters for CED planning is to implement, in the pre-operative phase, numerical models able to predict the drug distribution within the brain [34, 12]. However, despite the fact that several studies have been conducted in the field, a satisfying level of planning has not been achieved yet. Ehlers and Wagner [12] suggested that this could be due to a lack of consensus on model-parameter values (in particular for hydraulic permeability and effective diffusivity).

Since the drug flows through interstitial pathways between neurons, taking into account the brain micro-structure is essential to infer the physical properties that drive both the convective and diffusive flux [14]. Brain micro-structure can be retrieved exploiting electron microscopy (EM), which guarantees high resolution at neuron scale [24, 39]. For example, in [44] and [43], two different methodologies, inspired by consolidated work in the literature [32, 11], are proposed to compute the brain hydraulic permeability and the effective diffusivity starting from the axon diameter distribution (ADD) [26] computed from axon manual segmentation in EM images.

In this scenario, the goal of this work was to develop an automatic and accurate method for axon segmentation in EM images with the goal to automatically retrieving reliable ADDs. Following recent advancements in the literature, the proposed segmentation algorithm was based on deep fully-convolutional neural networks (FCNNs) and, in particular, on deep-residual learning networks (Resnets) [16]. The evaluation was performed in terms of:

- Axon-segmentation performance on the ISBI2012 challenge dataset [2]
- Comparison of the ADD obtained from the FCNN-based and the ground-truth axon segmentation.

The paper is organized as follows: Sec. 2 surveys axon segmentation strategies, with a focus on deep learning. Sec. 3 explains the proposed approach to axon segmentation in EM images and ADD computation from the segmented images. Sec. 4 deals with the experimental protocol used to test the proposed methodology. Results are presented in Sec. 5 and discussed in Sec. 6. Finally, strength and limitations of this work are reported in Sec. 7.

2 State of the art

In the last decades, axon segmentation in EM images was mainly based on image filtering and thresholding [29], and mathematical morphology [31].

More recently, with the spreading of high-computational-power computers and publicly-available large and labeled datasets[1], machine learning methods became the most common approach to axon segmentation. One of the first attempts at using machine learning for axon segmentation was proposed in [1]. A hierarchical segmentation procedure based on random forest (RF) and watershed segmentation was proposed for 3D segmentation of neural tissues in scanning EM volume data from rat retina. Similarly, RF was exploited in [22] and its probabilistic output was used in combination with axon geometrical properties to define a regular cost function that enforced gap completion via perceptual grouping constraints. A similar approach was used in [25], where dense correspondence across sections was exploited to resolve ambiguities in neuronal segmentation.

During the last years, deep learning, a subfield of machine learning based on deep neural networks (DNN), drew the attention of researchers in the field [27]. First examples include [20] and [28], where deep artificial neural networks were used. For example, in [41] graph-theory was adopted and a convolutional neural network (CNN) was used to infer graph weights. In [9] a CNN was used to directly obtain axon segmentation. The network had four convolutional layers, each one followed by a max pooling layer. A similar approach was exploited also in [13] and in [40]. All the three approaches performed segmentation via pixel classification, using two fully connected layers at the end of the convolutional path.

A further innovation was introduced with the use of FCNNs. In a FCNN, the fully connected layers are replaced by up-convolutional layers, allowing a faster and more precise axon localization with respect to approaches based on fully-connected-layer classification [30, 27]. In [37] a FCNN, which is known as U-Net due to its u-shaped architecture, was proposed outperforming all the previous approaches.

[1] (`http://brainiac2.mit.edu/isbi_challenge/home`)

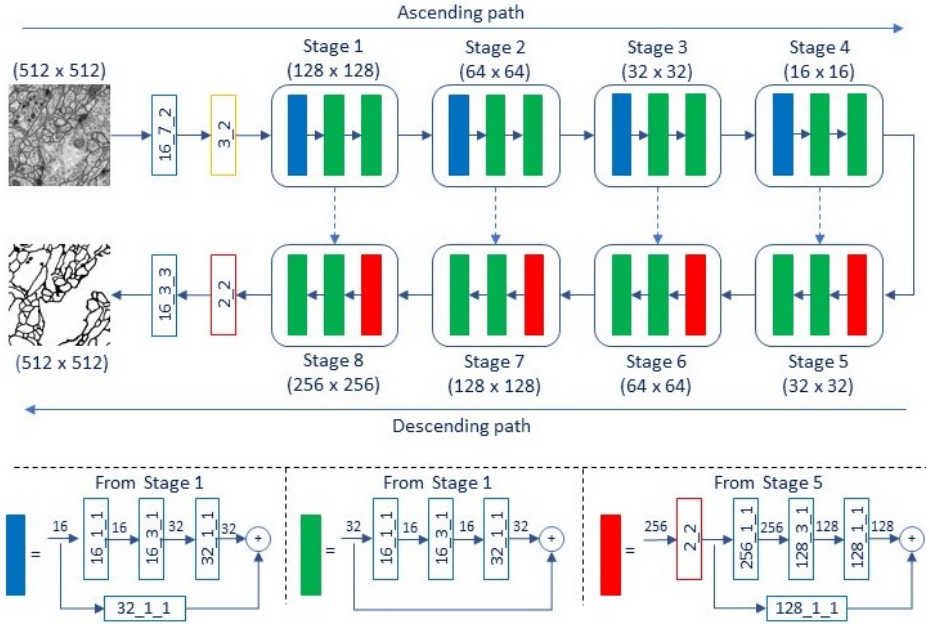

Fig. 1 Top: Scheme of the fully-convolutional neural network exploited in this work. There are four stages forming the descending path and four stages forming the ascending path. Each stage of the descending path is made of a convolutional block (full blue boxes) and two identity blocks (full green boxes), whereas in the ascending path the convolutional block is substituted by an upconvolutional block (full red boxes). We used the annotation introduced in [46], the empty blue boxes indicate convolutional layers (C_N_S) with channels C, kernel size $N \times N$ and stride S; the empty yellow box (N_S) indicates a maxpooling over $N \times N$ patches with stride S; the empty red boxes denote upsampling operation (K_K) with size K. Each convolutional operation is followed by batch normalization and a *ReLU* activation function. The dotted arrows refer to the concatenation of the feature map from the descending to the ascending path. Bottom: The convolutional and identity blocks of Stage 1, and the upconvolutional block of Stage 5 are shown. On the top of arrows, the number of feature maps is reported.

Starting from the U-Net implementation, architectural improvements mostly dealt with multilevel analysis (to encode image information at multiple scale) and introduction of residual blocks (to tackle the vanishing gradient problem) [33, 46]. In most of these approaches, remarkable performances were achieved at the cost of heavy time-consuming post-processing (e.g. based on superpixel and watershed segmentation for global refinement).

For our task, while post-processing may heavily prolong the overall computational time (i.e. the time for axon segmentation, ADD computation, and computation of the optimal CED infusion parameters with numerical models), methodologies based on residual blocks may be suitable for achieving a reasonable segmentation performance for computing ADDs from EM images.

3 Methods

3.1 Architecture description

As introduced in Sec. 1, the proposed FCNN architecture was inspired by U-Net [37] and Resnet [16]. As [37], the proposed FCNN consisted of a convolutional and an up-convolutional path. A schematic figure of the exploited FCNN architecture is shown in Fig. 1.

The proposed FCNN started with convolutions performed with 16 (7×7) filters followed by batch normalization, activation with the rectified linear unit and 2×2 pooling.

After this initial processing, in the convolutional path a first convolutional block was present with three convolutional kernels in cascade and a shortcut connection with 1×1 convolution for dimensional matching. The convolutional block was followed by two identity blocks made of three convolutional kernels and an identity skip connection. This structure (one convolutional block and two identity blocks) was repeated four times, doubling the number of convolutional kernels per layer. The up-convolutional path was symmetric to the convolutional one, but with up-convolutional blocks instead (thus halving the number of kernels per layer). All convolutions and up-convolutions were performed with 3×3 kernels. Batch normalization and activation with the rectified linear unit were applied after each convolution.

The proposed FCNN ended with a bare full convolution with two 3×3 kernels activated with a sigmoid function.

3.2 Training

Adam optimizer [23] was used to train the proposed FCNN. Adam exploited the first moment estimate ($\hat{m}_t$) and the second moment estimate ($\hat{v}_t$) of the loss-function gradient to update the network parameters:

$$\theta_{t+1,i} = \theta_{t,i} - \frac{\eta}{\sqrt{\hat{v}_t(g_{t,i})} + \epsilon} \cdot \hat{m}_t(g_{t,i}) \tag{1}$$

where $\theta_{t+1,i}$ denotes the i-th parameter after $t+1$ mini-batches, $g_{t,i}$ is the gradient with respect to the parameter θ_i after t mini-batches and ϵ is a small number. The cost function we adopted was the Dice similarity coefficient.

4 Experimental protocol

The dataset used to test the segmentation performance was released for the ISBI2012 challenge [2]. The training dataset is composed by 30 sections from the ventral nerve cord of a first-instar Drosophila larva acquired using serial section transmission EM. The 30 sections are 512×512 grayscale images. The ground-truth segmentation is composed by 512×512 binary images, where the axons membranes are labeled in black and the background is labeled in white. The ISBI2012 challenge

[2] (`http://brainiac2.mit.edu/isbi_challenge/home`)

organizers provided also another set of 30 (512 x 512) grayscale images (for which the ground truth was not publicly available) for testing purposes.

As suggested in [37] and in [13], data augmentation was performed. Seven linear transformations (rotations of 0°, 30°, 45°, 60° and 90°, vertical and horizontal mirroring) and eleven non-linear transformations (barrel transform, sinusoidal transform and shearing) were applied. The augmented dataset consisted of $8 \times 11 \times 30 = 2310$ training images.

The training and testing images were padded (symmetric padding) to compensate the pixel loss due to the convolution operations. This was the only manipulation we performed on the images during segmentation.

Adam optimizer parameters were set as suggested in [23]. We train the proposed FCNN with a batch size of 16 on 100 training epochs and initial learning rate of 10^{-3}. The 40% of the training images was used as validation set.

We performed all our experiments on Google Colaboratory[3].

To evaluate the segmentation performance of the proposed FCNN, we used the metrics suggested by the challenge organizer[4]

– **Foreground-restricted Rand Scoring (V^{Rand})**:

$$V^{Rand} = \frac{\sum_{ij} p_{ij}^2}{\alpha \sum_k s_k^2 + (1-\alpha) \sum_k t_k^2} \tag{2}$$

where p_{ij} is the probability that a randomly chosen pixel belongs to a segment i (defined as a set of connected pixels) in the predicted segmentation S and segment j in the ground-truth segmentation T, $s_i = \sum_j p_{ij}$ and $t_j = \sum_i p_{ij}$ are the probability that a randomly chosen pixel belongs to segment i in S and j in T respectively and $\alpha = 0.5$ is the Rand F-score which weights split and merge errors equally.

– **Information Theoretic Scoring (V^{Info})**:

$$V^{Info} = \frac{I(S;T)}{(1-\alpha)H(S) + \alpha H(T)} \tag{3}$$

where $I(S;T) = \sum_{ij} p_{ij} log(p_{ij}) - \sum_i s_i log(s_i) - \sum_j t_j log(t_j)$ is a measure of the similarity between S and T and $H(S) = -\sum_i s_i log(s_i)$ is the entropy.

The segmentation evaluation was performed through an automated online system where the segmented images were compared with the relative (hidden) ground-truth [13].

We compared the FCNN performances with those achieved by the best competitors in the literature among those that used the ISBI dataset for testing purposes, as to perform a fair comparison. In particular, we considered the FCNNs implemented in [46, 33, 5].

As introduced in Sec. 1, we compared the ADDs computed from the images segmented with the FCNN with those computed from the ground-truth images (ADD was computed as in [26]). As the ground-truth for the testing images of the ISBI dataset was not available, we divided the original training dataset in a

[3] https://colab.research.google.com/

[4] (`http://brainiac2.mit.edu/isbi_challenge/evaluation`)

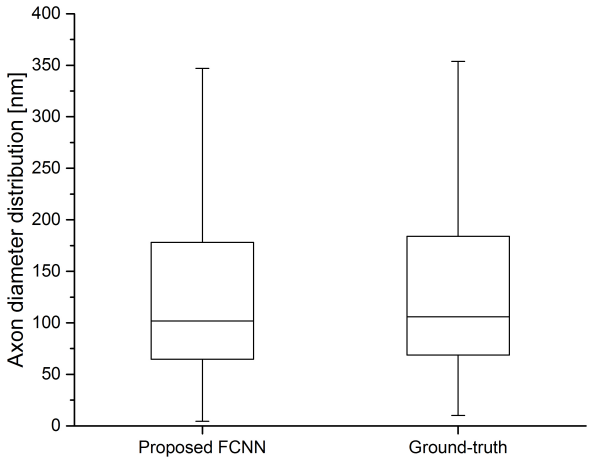

Fig. 2 Comparison between the axon diameter distributions extracted from the segmented and the ground-truth images.

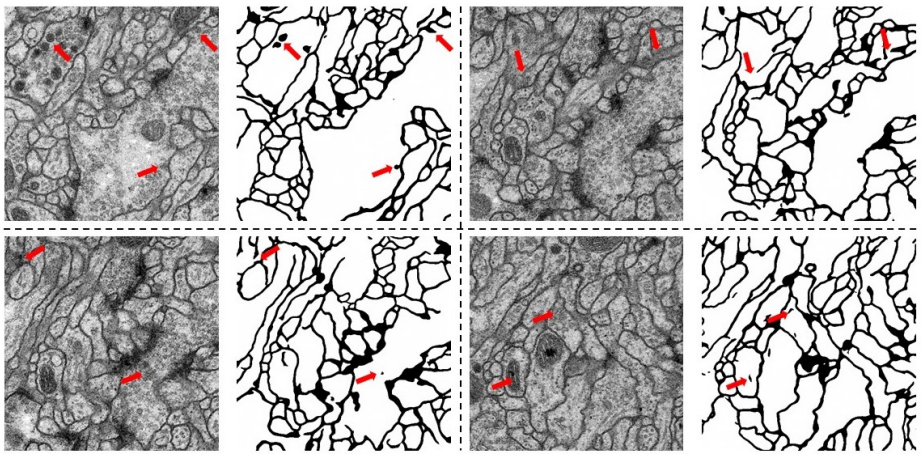

Fig. 3 Sample segmentation results obtained with the proposed FCNN. Raw testing images and output probability maps are compared. Red arrows on input images and output segmentation maps indicate structures that were incorrectly segmented.

subset for re-training from scratch the FCNN (20 images) and a set for computing the ADD (10 images). Both subsets underwent data augmentation (seven linear transformations and eleven non-linear transformations). The Wilcoxon rank-signed test (significance level = 0.05) was used to assess whether statistical differences existed between the ADDs computed from the FCNN-based segmentation and from the ground-truth.

Table 1 V_{Rand}, V_{Info} and training time for the proposed and the competitor approaches. The V_{Rand}, V_{Info} are computed on the testing set using the best FCNN model over the 100 training epochs.

Model	V_{Rand}	V_{Info}	Training time
Ref. [46]	0.983563573	0.990630782	36 hours
Ref. [5]	0.982616131	0.989461939	20 hours
Ref. [33]	0.980582825	0.988163049	-
Proposed	0.941987271	0.976824393	5 hours

5 Results

No significant differences were found when comparing the ADDs computed from the images segmented with the FCNN and the relevant ground truth (these results were obtained with a $V_{info} = 0.96$). The ADDs are shown in the boxplots in Fig. 2.

In Table 1, the V_{Rand} and V_{Info} obtained for the proposed FCNN and for the competing approaches are reported. Training time is reported, too.

The proposed FCNN architecture had a lower training time (5 hours) with respect to the competitors at the cost of a slightly lower performance (V_{Rand} = 0.941987271 and V_{Info} = 0.976824393). The computational time required to segment one image was 0.2 s with a non-optimized code. A direct comparison with the competitors was not possible though, as the relevant testing time was not reported.

Sample testing EM images and segmentation results after Otsu's thresholding, that we performed for visualization purpose only, are shown in Fig. 3.

6 Discussion

From Fig. 2, the achieved ADD was comparable (no statically significant difference were found) with that obtained with time-expensive manual tracing, thus indicating that the achieved segmentation performance was appropriate for our purposes. This was possible even if some errors were present in the segmentation, mainly due to thick axon borders and to small-organelle profiles within big axons (Fig. 3). False positive in correspondence of mitochondrial structures were detected, too. Errors were mainly related to intensity drops, noise in the images and limited number of samples against the high data variability.

In Table 1, it is possible to notice that the proposed FCNN achieved performances comparable with the competing approaches in terms of V_{Rand} and V_{Info} (the values were $4.1 \cdot 10^{-2}$ and $1.3 \cdot 10^{-2}$ lower, respectively, than those for [46], which achieved the best performances).

The time required for training our FCNN was significantly lower with respect to all the other competitor methods (about four times lower with respect to [5] and seven times lower with respect to [46]). Furthermore, even if the testing times are not reported by the competitors, they performed heavy post-processing that sharply increases the segmentation computational cost. On the contrary, our approach, without any post-processing, obtained good results as supported by the absence of significant difference between the ADDs extracted from the ground-truth and the proposed FCNN (Fig. 2).

A limitation of this work can be seen in the fact that our experimental protocol dealt with axons of Drosophila larva, instead of human ones. Nonetheless, while neuronal global architecture and axons diameter vary across different species, the axon microstructure (i.e., the round-shaped cross-section) is very similar [47].

With the goal of integrating this work into a full framework for reliable and robust fluid-dynamics brain-model implementation for CED, the FCNN performance should be tested on datasets of human-brain images. In fact, this work is part of the European project EDEN2020 (www.eden2020.eu), which supports the collections of such datasets, that, to the best of authors' knowledge, are currently not available. This could be attributed to the fact that high-resolution EM is a time consuming procedure. Images with lower resolution could be collected in a faster way (thus achieving a larger datasets and granting higher variability) but these images would probably be more challenging to segment. However, despite this still having to be experimentally tested, we expect that, with a proper training dataset, performance suitable for geometrical-parameter estimation can be still achieved. In fact, there is already evidence in other fields that proper segmentation performance may be achieved also when processing low-resolution images (e.g. [8]).

7 Conclusions

In this work, a method for accurate FCNN-based axon segmentation and ADD computation was proposed. The method was inspired by recent advancements in deep learning and integrated FCNNs and residual nets allowing good results in terms of axon geometrical-parameter extraction without the need of heavy post-processing (no statistically significant difference was found between the ADDs computed from the ground truth and proposed FCNN).

It is acknowledged that further research is required to ameliorate the proposed algorithm but the results presented in this work are surely a promising step toward CED optimization by means of brain micro-structure analysis.

Conflict of interest The authors have no conflict of interest to disclose.

Ethical standards This article does not contain any studies with human participants. All applicable international, national and/or institutional guidelines for the care and use of animals were followed.

Acknowledgements This project has received funding from the European Union's Horizon 2020 research and innovation programme under grant agreement No 688279.

References

1. Andres B, Köthe U, Helmstaedter M, Denk W, Hamprecht FA (2008) Segmentation of SBFSEM volume data of neural tissue by hierarchical classification. In: Joint Pattern Recognition Symposium, Springer, pp 142–152
2. Arganda-Carreras I, Turaga SC, Berger DR, Cireşan D, Giusti A, Gambardella LM, Schmidhuber J, Laptev D, Dwivedi S, Buhmann JM, Liu T, Seyedhosseini M, Tasdizen T, Kamentsky L, Burget R, Uher V, Tan X, Sun C, Pham TD, Bas

E, Uzunbas MG, Cardona A, Schindelin J, Seung SH (2015) Crowdsourcing the creation of image segmentation algorithms for connectomics. Frontiers in Neuroanatomy 9:142
3. Barua N, Lowis S, Woolley M, OSullivan S, Harrison R, Gill S (2013) Robot-guided convection-enhanced delivery of carboplatin for advanced brainstem glioma. Acta Neurochirurgica 155(8):1459–1465
4. Barua NU, Hopkins K, Woolley M, OSullivan S, Harrison R, Edwards RJ, Bienemann AS, Wyatt MJ, Arshad A, Gill SS (2016) A novel implantable catheter system with transcutaneous port for intermittent convection-enhanced delivery of carboplatin for recurrent glioblastoma. Drug Delivery 23(1):167–173
5. Beier T, Pape C, Rahaman N, Prange T, Berg S, Bock DD, Cardona A, Knott GW, Plaza SM, Scheffer LK, Koethe U, Kreshuk A, Hamprecht FA (2017) Multicut brings automated neurite segmentation closer to human performance. Nature Methods 14(2):101
6. Bobo RH, Laske DW, Akbasak A, Morrison PF, Dedrick RL, Oldfield EH (1994) Convection-enhanced delivery of macromolecules in the brain. Proceedings of the National Academy of Sciences 91(6):2076–2080
7. Buckner JC, Brown PD, O'neill BP, Meyer FB, Wetmore CJ, Uhm JH (2007) Central nervous system tumors. In: Mayo Clinic Proceedings, Elsevier, vol 82, pp 1271–1286
8. Cai D, Chen K, Qian Y, Kämäräinen JK (2017) Convolutional low-resolution fine-grained classification. Pattern Recognition Letters
9. Ciresan D, Giusti A, Gambardella LM, Schmidhuber J (2012) Deep neural networks segment neuronal membranes in electron microscopy images. In: Advances in Neural Information Processing Systems, pp 2843–2851
10. Debinski W, Tatter SB (2009) Convection-enhanced delivery for the treatment of brain tumors. Expert Review of Neurotherapeutics 9(10):1519–1527
11. Dias M, Fernandes P, Guedes J, Hollister S (2012) Permeability analysis of scaffolds for bone tissue engineering. Journal of Biomechanics 45(6):938–944
12. Ehlers W, Wagner A (2015) Multi-component modelling of human brain tissue: a contribution to the constitutive and computational description of deformation, flow and diffusion processes with application to the invasive drug-delivery problem. Computer Methods in Biomechanics and Biomedical Engineering 18(8):861–879
13. Fakhry A, Peng H, Ji S (2016) Deep models for brain EM image segmentation: novel insights and improved performance. Bioinformatics 32(15):2352–2358
14. Goriely A, Geers MG, Holzapfel GA, Jayamohan J, Jérusalem A, Sivaloganathan S, Squier W, van Dommelen JA, Waters S, Kuhl E (2015) Mechanics of the brain: perspectives, challenges, and opportunities. Biomechanics and Modeling in Mechanobiology 14(5):931–965
15. Hanif F, Muzaffar K, Perveen K, Malhi SM, Simjee SU (2017) Glioblastoma multiforme: A review of its epidemiology and pathogenesis through clinical presentation and treatment. Asian Pacific Journal of Cancer Prevention 18(1):3
16. He K, Zhang X, Ren S, Sun J (2016) Deep residual learning for image recognition. In: IEEE Conference on Computer Vision and Pattern Recognition, pp 770–778
17. Iacob G, Dinca EB (2009) Current data and strategy in glioblastoma multiforme. Journal of Medicine and Life 2(4):386

18. Jahangiri A, Chin AT, Flanigan PM, Chen R, Bankiewicz K, Aghi MK (2017) Convection-enhanced delivery in glioblastoma: a review of preclinical and clinical studies. Journal of Neurosurgery 126(1):191–200
19. Jovčevska I, Kočevar N, Komel R (2013) Glioma and glioblastoma-how much do we (not) know? Molecular and Clinical Oncology 1(6):935–941
20. Jurrus E, Paiva AR, Watanabe S, Anderson JR, Jones BW, Whitaker RT, Jorgensen EM, Marc RE, Tasdizen T (2010) Detection of neuron membranes in electron microscopy images using a serial neural network architecture. Medical Image Analysis 14(6):770–783
21. Kanu OO, Mehta A, Di C, Lin N, Bortoff K, Bigner DD, Yan H, Adamson DC (2009) Glioblastoma multiforme: a review of therapeutic targets. Expert Opinion on Therapeutic Targets 13(6):701–718
22. Kaynig V, Fuchs T, Buhmann JM (2010) Neuron geometry extraction by perceptual grouping in SSTEM images. In: IEEE Conference on Computer Vision and Pattern Recognition, IEEE, pp 2902–2909
23. Kingma D, Ba J (2014) Adam: A method for stochastic optimization. arXiv preprint arXiv:14126980
24. Knott G, Genoud C (2013) Is EM dead? J Cell Sci 126(20):4545–4552
25. Laptev D, Vezhnevets A, Dwivedi S, Buhmann JM (2012) Anisotropic sstem image segmentation using dense correspondence across sections. In: International Conference on Medical Image Computing and Computer-Assisted Intervention, Springer, pp 323–330
26. Liewald D, Miller R, Logothetis N, Wagner HJ, Schüz A (2014) Distribution of axon diameters in cortical white matter: an electron-microscopic study on three human brains and a macaque. Biological cybernetics 108(5):541–557
27. Litjens G, Kooi T, Bejnordi BE, Setio AAA, Ciompi F, Ghafoorian M, van der Laak JA, van Ginneken B, Sánchez CI (2017) A survey on deep learning in medical image analysis. arXiv preprint arXiv:170205747
28. Liu T, Jurrus E, Seyedhosseini M, Ellisman M, Tasdizen T (2012) Watershed merge tree classification for electron microscopy image segmentation. In: IEEE International Conference on Pattern Recognition, IEEE, pp 133–137
29. Mishchenko Y (2009) Automation of 3D reconstruction of neural tissue from large volume of conventional serial section transmission electron micrographs. Journal of Neuroscience Methods 176(2):276–289
30. Moccia S, De Momi E, El Hadji S, Mattos LS (2018) Blood vessel segmentation algorithms–Review of methods, datasets and evaluation metrics. Computer Methods and Programs in Biomedicine 158:71–91
31. More HL, Chen J, Gibson E, Donelan JM, Beg MF (2011) A semi-automated method for identifying and measuring myelinated nerve fibers in scanning electron microscope images. Journal of Neuroscience Methods 201(1):149–158
32. Nicholson C, Hrabětová S (2017) Brain extracellular space: the final frontier of neuroscience. Biophysical Journal
33. Quan TM, Hildebrand DG, Jeong WK (2016) Fusionnet: A deep fully residual convolutional neural network for image segmentation in connectomics. arXiv preprint arXiv:161205360
34. Raghavan R, Brady M (2011) Predictive models for pressure-driven fluid infusions into brain parenchyma. Physics in Medicine and Biology 56(19):6179
35. Raghavan R, Brady ML, Rodríguez-Ponce MI, Hartlep A, Pedain C, Sampson JH (2006) Convection-enhanced delivery of therapeutics for brain disease, and

its optimization. Neurosurgical Focus 20(4):E12
36. Raghavan R, Brady ML, Sampson JH (2016) Delivering therapy to target: improving the odds for successful drug development
37. Ronneberger O, Fischer P, Brox T (2015) U-net: Convolutional networks for biomedical image segmentation. In: International Conference on Medical Image Computing and Computer-Assisted Intervention, Springer, pp 234–241
38. Thakkar JP, Dolecek TA, Horbinski C, Ostrom QT, Lightner DD, Barnholtz-Sloan JS, Villano JL (2014) Epidemiologic and molecular prognostic review of glioblastoma. Cancer Epidemiology and Prevention Biomarkers 23(10):1985–1996
39. Titze B, Genoud C (2016) Volume scanning electron microscopy for imaging biological ultrastructure. Biology of the Cell 108:307–323
40. Tschopp F, Martel JN, Turaga SC, Cook M, Funke J (2016) Efficient convolutional neural networks for pixelwise classification on heterogeneous hardware systems. In: IEEE International Symposium on Biomedical Imaging, IEEE, pp 1225–1228
41. Turaga SC, Murray JF, Jain V, Roth F, Helmstaedter M, Briggman K, Denk W, Seung HS (2010) Convolutional networks can learn to generate affinity graphs for image segmentation. Neural Computation 22(2):511–538
42. Varenika V, Dickinson P, Bringas J, LeCouteur R, Higgins R, Park J, Fiandaca M, Berger M, Sampson J, Bankiewicz K (2008) Detection of infusate leakage in the brain using real-time imaging of convection-enhanced delivery. Journal of Neurosurgery 109(5):874–880
43. Vidotto M, Dini D, De Momi E (2018) Effective diffusion and tortuosity in brain white matter. In: International Conference the IEEE Engineering in Medicine and Biology Society
44. Vidotto M, Gazzara M, Botnariuc D, Bernardini A, Dini D, De Momi E (2018) White matter hydraulic permeability from electron microscopy images. In: World Congress of Biomechanics
45. White E, Bienemann A, Malone J, Megraw L, Bunnun C, Wyatt M, Gill S (2011) An evaluation of the relationships between catheter design and tissue mechanics in achieving high-flow convection-enhanced delivery. Journal of Neuroscience Methods 199(1):87–97
46. Xiao C, Liu J, Chen X, Han H, Shu C, Xie Q (2018) Deep contextual residual network for electron microscopy image segmentation in connectomics. In: International Symposium on Biomedical Imaging, IEEE, pp 378–381
47. Zaimi A, Wabartha M, Herman V, Antonsanti PL, Perone CS, Cohen-Adad J (2018) Axondeepseg: automatic axon and myelin segmentation from microscopy data using convolutional neural networks. Scientific reports 8(1):3816